# Trinodal Self-Penetrating Nets from Reactions of 1,4-Bis(alkoxy)-2,5-bis(3,2′:6′,3″-terpyridin-4′-yl)benzene Ligands with Cobalt(II) Thiocyanate

**Giacomo Manfroni [1], Alessandro Prescimone [1] , Stuart R. Batten [2], Y. Maximilian Klein [3] ,**
**Dariusz J. Gawryluk [3] , Edwin C. Constable [1] and Catherine E. Housecroft [1],\* **

[1] Department of Chemistry, University of Basel, BPR 1096, Mattenstrasse 24a, CH-4058 Basel, Switzerland; giacomo.manfroni@unibas.ch (G.M.); alessandro.prescimone@unibas.ch (A.P.); edwin.constable@unibas.ch (E.C.C.)
[2] School of Chemistry, Monash University, Victoria 3800, Australia; stuart.batten@monash.edu
[3] Laboratory for Multiscale Materials Experiments, Paul Scherrer Institut, CH-5232 Villigen PSI, Switzerland; maximilian.klein@psi.ch (Y.M.K.); dariusz.gawryluk@psi.ch (D.J.G.)
\* Correspondence: catherine.housecroft@unibas.ch; Tel.: +41-61-207-1008

**Abstract:** The tetratopic ligands 1,4-bis(2-ethylbutoxy)-2,5-bis(3,2′:6′,3″-terpyridin-4′-yl)benzene (**1**) and 1,4-bis(3-methylbutoxy)-2,5-bis(3,2′:6′,3″-terpyridin-4′-yl)benzene (**2**) have been prepared and characterized by $^1H$ and $^{13}C\{^1H\}$ NMR, IR, and absorption spectroscopies and mass spectrometry. Reactions of **1** and **2** with cobalt(II) thiocyanate under conditions of crystal growth at room temperature result in the formation of $[\{Co(\mathbf{1})(NCS)_2\}\cdot MeOH\cdot 3CHCl_3]_n$ and $[\{Co(\mathbf{2})(NCS)_2\}\cdot 0.8MeOH\cdot 1.8CHCl_3]_n$. Single-crystal X-ray diffraction reveals that each crystal lattice consists of a trinodal self-penetrating $(6^2.8^4)(6^4.8^2)(6^5.8)_2$ net. The nodes are defined by two independent cobalt centres and the centroids of two crystallographically independent ligands which are topologically equivalent.

**Keywords:** three-dimensional network; self-penetration; 3,2′:6′,3″-terpyridine; tetratopic ligand; cobalt(II) thiocyanate

## 1. Introduction

The coordination chemistry of 2,2′:6′,2″-terpyridine (2,2′:6′,2″-tpy, preferred IUPAC name $1^2,2^2:2^6,3^2$-terpyridine) is well established and is dominated by chelation to a single metal centre [1,2], with mono or bidentate modes being less common [3]. As Scheme 1 shows, tridentate bonding by 2,2′:6′,2″-tpy is synonymous with binding one metal ion and the ligand is classed as monotopic (having a single metal-binding domain) [4]. The incorporation of two or more 2,2′:6′,2″-tpy units into a single organic molecule leads to a multitopic ligand [2,5–7] and is a design strategy that has been used to access high nuclearity coordination assemblies [8–10]. An alternative approach is to use isomers of terpyridine, such as 3,2′:6′,3″-tpy (PIN $1^3,2^2:2^6,3^3$-terpyridine) and 4,2′:6′,4″-tpy (PIN $1^4,2^2:2^6,3^4$-terpyridine), in which chelation is not possible (Scheme 1). Both 3,2′:6′,3″-tpy and 4,2′:6′,4″-tpy coordinate to metal ions through only the outer nitrogen atoms and are therefore ditopic ligands [4] with two discrete pyridine metal-binding domains. Connection of two 3,2′:6′,3″-tpy or 4,2′:6′,4″-tpy domains through a spacer leads to tetratopic ligands with four discrete pyridine metal-binding domains (Scheme 2), which are suitable as building blocks for 2D- and 3D-coordination networks [4,11–18].
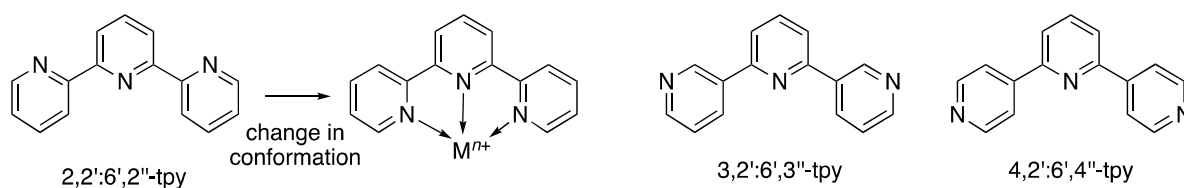
**Scheme 1.** Conformational change for monotopic 2,2′:6′,2″-tpy as it binds a metal ion, and the structures of 3,2′:6′,3″-tpy and 4,2′:6′,4″-tpy.
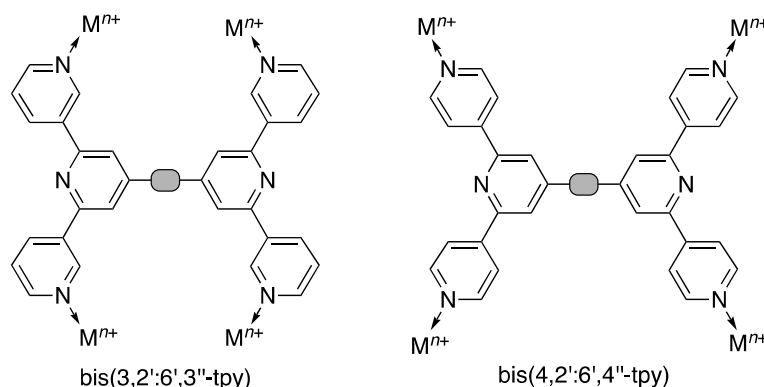


**Scheme 2.** Connection of two 3,2′:6′,3″-tpy or 4,2′:6′,4″-tpy domains through a spacer gives tetratopic ligands.

Despite the fact that Cave and Raston reported the synthesis of bis(4,2′:6′,4″-terpyridin-4′-yl)benzene in 2001 [19], the coordination chemistry of bis(4,2′:6′,4″-tpy) ligands has only developed significantly in the last few years. With phenylene spacers, the ligands are only poorly soluble [16,20], but the introduction of solubilizing alkoxy substituents increases solubility in $CHCl_3$ and allows the development of a versatile toolbox of functionalities for tuning their electronic and steric properties. We have recently reviewed our own progress in the coordination chemistry of ditopic and tetratopic ligands with 4,2′:6′,4″-tpy metal-binding domains [21]. The coordination behavior of bis(3,2′:6′,3″-tpy) remains little explored [13,22]. Rotation about the inter-ring C–C bonds in 3,2′:6′,3″-tpy (shown in red in Scheme 3) results in conformational changes that, in turn, define the vectorial arrangement of the nitrogen lone pairs in the metal-binding domains (Scheme 3). This results in bis(3,2′:6′,3″-tpy) ligands being especially flexible building blocks for the assembly of 2D- and 3D-networks. Here, we report the synthesis and characterization of two bis(3,2′:6′,3″-tpy) ligands **1** and **2** (Scheme 4) and their reactions with cobalt(II) thiocyanate to assemble self-penetrating 3D-frameworks.
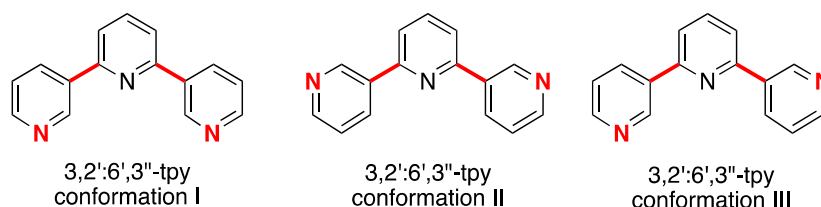


**Scheme 3.** Some of the possible conformations that a 3,2′:6′,3″-tpy unit can adopt by virtue of rotations about the transannular C–C bonds (shown in red). 3,2′:6′,3″-tpy coordinates only through the outer (red) N atoms.
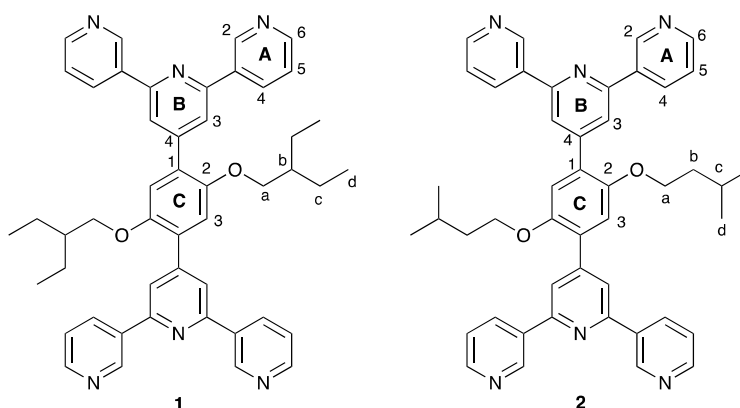
**Scheme 4.** Structures of ligands **1** and **2** with atom labels used for NMR spectroscopic assignments.

## 2. Materials and Methods

### 2.1. General

$^1$H and $^{13}$C{$^1$H} NMR spectra were recorded on a Bruker Avance III-500 spectrometer (Bruker BioSpin AG, Fällanden, Switzerland) at 298 K. The $^1$H and $^{13}$C NMR chemical shifts were referenced with respect to residual solvent peaks ($\delta$ TMS = 0). Matrix-assisted laser desorption ionization time-of-flight (MALDI-TOF) mass spectra were recorded on a Shimadzu MALDI 8020 (Shimadzu Schweiz GmbH, 4153 Reinach, Switzerland) using α-cyano-4-hydroxycinnamic acid as the matrix. Electrospray ionization (ESI) mass spectra were recorded using a Shimadzu LCMS-2020 instrument (Shimadzu Schweiz GmbH, Reinach, Switzerland). Samples were introduced as 200–800 μM solutions in MeOH, in some cases with NaCl added. High resolution electrospray (HR-ESI) mass spectra were measured on a Bruker maXis 4G QTOF instrument (Bruker BioSpin AG, Fällanden, Switzerland). PerkinElmer UATR Two (Perkin Elmer, 8603 Schwerzenbach, Switzerland) and Cary-5000 (Agilent Technologies Inc., Santa Clara, CA, US) instruments were used to record FT-infrared (IR) and UV-VIS absorption spectra, respectively.

Commercial chemicals were 3-acetylpyridine from Acros Organics (Chemie Brunschwig AG, 4052 Basel, Switzerland), 2,5-dibromohydroquinone from Tokyo Chemical Industry (4-10-2 Nihonbashi-honcho, Chuo-ku, Tokyo 103-0023, Japan), and Co(NCS)$_2$ from Sigma Aldrich (Sigma Aldrich Chemie GmbH, 89555 Steinheim, Germany). These chemicals were used as received.

### 2.2. 1,4-Dibromo-2,5-bis(2-ethylbutoxy)benzene

Dry DMF (30 mL) was added to a mixture of anhydrous K$_2$CO$_3$ (2.19 g, 15.8 mmol), 2,5-dibromohydroquinone (1.50 g, 5.6 mmol) and 1-bromo-2-ethylbutane (2.31 g, 14.0 mmol). The solution was heated (with stirring) to 100 °C under N$_2$ for 18 h. The mixture was cooled to room temperature, poured onto ice/water (100 mL), and stirred for 20 min. The resulting suspension was extracted with CH$_2$Cl$_2$ (3 × 75 mL) and then the volume was reduced and dried in vacuo for 15 h at 45 °C to yield 1,4-dibromo-2,5-bis(2-ethylbutoxy)benzene as a dark brown oil (2.33 g, 5.34 mmol, 95.4%). $^1$H NMR (500 MHz, CDCl$_3$) $\delta$/ppm 7.08 (s, 2H, H$^3$), 3.84 (d, *J* = 5.6 Hz, 4H, H$^a$), 1.77–1.63 (m, 2H, H$^b$), 1.58–1.43 (m, 8H, H$^c$), 0.94 (t, *J* = 7.5 Hz, 12H, H$^d$). $^{13}$C{$^1$H} NMR (126 MHz, CDCl$_3$) $\delta$/ppm 150.3 (C$^2$), 118.4 (C$^3$), 111.2 (C$^1$), 72.3 (C$^a$), 41.1 (C$^b$), 23.5 (C$^c$), 11.3 (C$^d$). MALDI-TOF-MS *m/z* 436.04 [M+H]$^+$ (calc. 436.04).

### 2.3. 2,5-Bis(2-ethylbutoxy)benzene-1,4-dicarbaldehyde

1,4-Dibromo-2,5-bis(2-ethylbutoxy)benzene (1.50 g, 3.4 mmol) was dissolved in dry Et$_2$O (100 mL) and a solution of *n*-BuLi in *n*-hexane (1.6 M, 6.5 mL, 10.0 mmol) was added slowly at 0 °C under an N$_2$ atmosphere over a period of 15 min. After 2 h, dry DMF (0.80 mL, 10.0 mmol) was added to

the white suspension. The mixture was stirred for one day under $N_2$ while warming from 0 °C to room temperature. The reaction mixture was neutralized with saturated aqueous $NH_4Cl$ solution and extracted with $CH_2Cl_2$ (150 mL). The organic layers were dried over $MgSO_4$ and concentrated in vacuo. The product was obtained as a yellow oil (1.15 g, 3.40 mmol, 100%). $^1$H NMR (500 MHz, CDCl$_3$) $\delta$/ppm 10.52 (s, 2H, H$^{CHO}$), 7.44 (s, 2H, H$^3$), 3.99 (d, $J$ = 5.6 Hz, 4H, H$^a$), 1.77–1.68 (m, 2H, H$^b$), 1.54–1.45 (m, 8H, H$^c$), 0.94 (t, $J$ = 7.5 Hz, 12H, H$^d$). $^{13}$C{$^1$H} NMR (126 MHz, CDCl$_3$) $\delta$/ppm 189.5 (C$^{CHO}$), 155.6 (C$^2$), 129.5 (C$^1$), 111.7 (C$^3$), 71.3 (C$^a$), 41.1 (C$^b$), 23.6 (C$^c$), 11.30 (C$^d$). MALDI-TOF-MS *m/z* 336.17 [M+2H]$^+$ (calc. 336.23); ESI-MS (MeOH, NaCl) 421.21 [M+2MeOH+Na]$^+$ (calc. 421.26), 389.20 [M+MeOH+Na]$^+$ (base peak, calc. 389.23).

### 2.4. 2,5-Bis(3-methylbutoxy)benzene-1,4-dicarbaldehyde

2,5-Bis(3-methylbutoxy)benzene-1,4-dicarbaldehyde has previously been reported [23,24]. It was prepared in the same manner as 2,5-bis(2-ethylbutoxy)benzene-1,4-dicarbaldehyde, and the $^1$H and $^{13}$C{$^1$H} NMR data were in accord with published data [23,24].

### 2.5. Synthesis of 1,4-Bis(2-ethylbutoxy)-2,5-bis(3,2′:6′,3″-terpyridin-4′-yl)benzene (**1**)

2,5-Bis(2-ethylbutoxy)benzene-1,4-dicarbaldehyde (570 mg, 1.7 mmol) was dissolved in EtOH (50 mL). 3-Acetylpyridine (927 mg, 0.84 mL, 7.65 mmol) was added followed by crushed KOH (429 mg, 7.65 mmol) in one portion. Aqueous $NH_3$ solution (30%, 14.3 mL) was slowly added and the reaction mixture was stirred at room temperature for three days. The solid that formed was collected by decantation, washed with water (3 × 10 mL) and ethanol (3 × 10 mL) and then dried in vacuo overnight. The product was isolated as a light-yellow powder (317 mg, 0.43 mmol, 25.2%). M.p. = 209–212 °C. $^1$H NMR (500 MHz, CDCl$_3$) $\delta$/ppm 9.39 (dd, $J$ = 2.3, 0.9 Hz, 4H, H$^{A2}$), 8.72 (dd, $J$ = 4.7, 1.7 Hz, 4H, H$^{A6}$), 8.54 (m, 4H, H$^{A4}$), 8.02 (s, 4H, H$^{B3}$), 7.48 (m, 4H, H$^{A5}$), 7.17 (s, 2H, H$^{C3}$), 3.95 (d, $J$ = 5.5 Hz, 4H, H$^a$), 1.65–1.58 (m, 2H, H$^b$), 1.42–1.32 (m, 8H, H$^c$), 0.82 (t, $J$ = 7.5 Hz, 12H, H$^d$). $^{13}$C{$^1$H} NMR (500 MHz, CDCl$_3$) $\delta$/ppm 154.8 (C$^{B2}$), 150.8 (C$^{C2}$), 150.4 (C$^{A6}$), 148.5 (C$^{A2}$), 148.2 (C$^{C1}$), 134.8 (C$^{A3}$), 134.6 (C$^{A4}$), 129.5 (C$^{B4}$), 123.8 (C$^{A5}$), 120.4 (C$^{B3}$), 115.2 (C$^{C3}$), 71.7 (C$^a$), 41.3 (C$^b$), 23.6 (C$^c$), 11.3 (C$^d$). UV-VIS (CHCl$_3$, 1.2 × 10$^{-5}$ mol dm$^{-3}$) $\lambda$/nm 244 ($\varepsilon$/dm$^3$ mol$^{-1}$ cm$^{-1}$ 52,000) 278 sh (42,300), 318 (18,100), 354 (9,800). MALDI-TOF-MS *m/z* 741.34 [M+H]$^+$ (calc. 741.39). Found C 77.25, H 6.56, N 11.03; required for $C_{48}H_{48}N_6O_2$ C 77.81, H 6.53, N 11.34. The FT-IR spectrum of **1** is shown in Figure S1 (see Supplementary material).

### 2.6. Synthesis of 1,4-Bis(3-methylbutoxy)-2,5-bis(3,2′:6′,3″-terpyridin-4′-yl)benzene (**2**)

2,5-Bis(3-methylbutoxy) benzene-1,4-dicarbaldehyde (510 mg, 1.66 mmol) was dissolved in 30 mL EtOH (30 mL) and then 3-acetylpyridine (905 mg, 0.82 mL, 7.47 mmol) was added. Crushed KOH (419 mg, 7.47 mmol) was then added in one portion. Aqueous $NH_3$ solution (30%, 12.8 mL) was slowly added and the reaction mixture was stirred at room temperature for one day. The solid that formed was collected by filtration, washed with water (3 × 10 mL) and ethanol (3 × 10 mL) and then dried in vacuo for three days. The product was isolated as a slightly yellowish powder (207 mg, 0.29 mmol, 17.5%). M.p. = 220–221 °C. $^1$H NMR (500 MHz, CDCl$_3$) $\delta$/ppm 9.38 (dd, $J$ = 2.3, 0.9 Hz, 4H, H$^{A2}$), 8.72 (dd, $J$ = 4.7, 1.7 Hz, 4H, H$^{A6}$), 8.53 (dt, $J$ = 8.0, 2.0 Hz, 4H, H$^{A4}$), 8.03 (s, 4H, H$^{B3}$), 7.48 (ddd, $J$ = 8.0, 4.8, 0.9 Hz, 4H, H$^{A5}$), 7.17 (s, 2H, H$^{C3}$), 4.09 (t, $J$ = 6.4 Hz, 4H, H$^a$), 1.79–1.71 (m, 2H, H$^c$), 1.66 (m, 4H, H$^b$), 0.86 (d, $J$ = 6.6 Hz, 12H, H$^d$). $^{13}$C{$^1$H} NMR (500 MHz, CDCl$_3$) $\delta$/ppm 154. (C$^{B2}$), 150.71 (C$^{C2}$), 150.4 (C$^{A6}$), 148.5 (C$^{A2}$), 148.1 (C$^{C1}$), 134.9 (C$^{A3}$), 134.6 (C$^{A4}$), 129.4 (C$^{B4}$), 123.8 (C$^{A5}$), 120.4 (C$^{B3}$), 115.3 (C$^{C3}$), 68.1 (C$^a$), 38.2 (C$^b$), 25.2 (C$^c$), 22.6 (C$^d$). UV-VIS (CHCl$_3$, 1.0 × 10$^{-5}$ mol dm$^{-3}$) $\lambda$/nm 244 ($\varepsilon$/dm$^3$ mol$^{-1}$ cm$^{-1}$ 44,600) 279 sh (36,200), 318 (16,500), 354 (9,800). MALDI-TOF-MS *m/z* 713.41 [M+H]$^+$ (calc. 713.36). HR-MS *m/z* 713.3587 [M+H]$^+$ (calc. 713.3599), 357.1836 [M+2H]$^{2+}$ (calc. 357.1836). Satisfactory elemental analysis could not be obtained. The FT-IR spectrum of **2** is shown in Figure S2 (see Supplementary material).

## 2.7. Synthesis of [{Co(**1**)(NCS)$_2$}·MeOH·3CHCl$_3$]$_n$

A MeOH (8 mL) solution of Co(NCS)$_2$ (1.75 mg, 0.01 mmol) was layered over a CHCl$_3$ (5 mL) solution of ligand **1** (7.41 mg; 0.01 mmol) in a crystallization tube (inner dimeter = 13.6 mm, volume = 24 mL). This was left to stand at room temperature. Orange block-like crystals visible to the eye were first obtained after 15 days, and a single crystal was selected for X-ray diffraction after another four days. A portion of the remaining crystals was mounted wet in a sample holder (to avoid loss of solvent from the crystals) and analyzed by powder X-ray diffraction (PXRD).

## 2.8. Synthesis of [{Co(**2**)(NCS)$_2$}·0.8MeOH·1.8CHCl$_3$]$_n$

A MeOH (8 mL) solution of Co(NCS)$_2$ (1.75 mg, 0.01 mmol) was layered over a CHCl$_3$ (5 mL) solution of ligand **2** (6.33 mg, 0.01 mmol) in a crystallization tube (inner dimeter = 13.6 mm, volume = 24 mL) which was left to stand at room temperature. Orange block-like crystals visible to the eye were first obtained after seven days, and an X-ray quality crystal was selected after two months. A portion of the remaining crystals was mounted wet in a sample holder (to avoid loss of solvent from the crystals) and analyzed by PXRD.

## 2.9. Crystallography

Single crystal data were collected on a Bruker APEX-II diffractometer (CuK$\alpha$ radiation) with data reduction, solution and refinement using the programs APEX, ShelXT, Olex2 and ShelXL v. 2014/7, or using a STOE StadiVari diffractometer equipped with a Pilatus300K detector and with a Metaljet D2 source (GaK$\alpha$ radiation) [25–28]. The structure was solved using Superflip and Olex2 [27,29,30]. The model was refined with ShelXL v. 2014/7 [28]. Structure analysis used Mercury CSD v. 4.2.0 [31,32].

In [{Co(**1**)(NCS)$_2$}·MeOH·3CHCl$_3$]$_n$, one CHCl$_3$ molecule was located and refined, and the Olex2 implementation of SQUEEZE [33] was used to treat the rest of the solvent region. A solvent mask was calculated, and 1044.0 electrons were found in a volume of 3742.0 Å$^{-3}$ in one void. This is consistent with the presence of 2CHCl$_3$ and 1CH$_3$OH per formula unit which account for 1072.0 electrons. The formulae and dependent numbers were adapted to account for this. Due to their thermal motion, the aliphatic chains had to be heavily restrained with SIMU, SADI, and DFIX restraints and were refined isotropically. H atoms were positioned geometrically, then allowed to ride on their parent atom.

In [{Co(**2**)(NCS)$_2$}·0.8MeOH·1.8CHCl$_3$]$_n$, the aliphatic chains display orientational and vibrational disorder and were modelled with the use of SADI and DFIX restraints, one chain over two sites of partial occupancies 0.60/0.40 and the other chain with equal occupancy sites. Some atoms were refined isotropically. Disorder in one thiocyanate ligand was modelled with two sites for the S atom of partial occupancies 0.75/0.25. All the solvent molecules present in this structure were modelled with partial occupancies. H atoms were positioned geometrically, then allowed to ride on their parent atoms.

Phase purity of bulk samples of the two compounds was confirmed at room temperature by PXRD in transmission mode using a Stoe Stadi P diffractometer equipped with a Cu K$\alpha$1 radiation (Ge(111) monochromator) and a DECTRIS MYTHEN 1K detector. The single crystal of [{Co(**1**)(NCS)$_2$}·MeOH·3CHCl$_3$]$_n$ is representative of the main phase of the bulk sample. Minor phases are also present in the bulk, which can be attributed to solvent loss during sample preparation and measurement. The bulk sample of [{Co(**2**)(NCS)$_2$}·0.8MeOH·1.8CHCl$_3$]$_n$ corresponds to the material characterized in the single crystal structure. The reflections of the main phases were indexed with a monoclinic cell in the space group *C*2/*c* (No. 15). The whole-pattern decomposition (profile matching) analysis of the diffraction patterns was done by the package FULLPROF SUITE [34–37] (version July-2019) using a previously determined instrumental resolution function (based on the silicon NIST standard 640d). The crystal model for the two compounds was taken from the single crystal diffraction data. Refined parameters were zero shift, sample displacement, transparency, lattice parameters, and peaks shapes (Y) as a Thompson-Cox-Hastings pseudo-Voigt function.

## 2.10. [{Co(**1**)(NCS)$_2$}·MeOH·3CHCl$_3$]$_n$

$C_{54}Cl_9CoH_{54}N_8O_3S_2$, $M_r$ = 1305.15, orange block, monoclinic, space group *C*2/*c*, *a* = 37.514(3), *b* = 17.4813(11), *c* = 26.6265(17) Å, *β* = 133.660(3)°, *V* = 12632.4(15) Å$^3$, $D_c$ = 1.373 g cm$^{-3}$, *T* = 130 K, *Z* = 8, *Z'* = 1, µ(CuKα) = 6.630 mm$^{-1}$. Total 69,524 reflections, 9110 unique ($R_{int}$ = 0.02879). Refinement of 5412 reflections (552 parameters) with *I* > 2*σ*(*I*) converged at final $R_1$ = 0.1118 ($R_1$ all data = 0.1470), $wR_2$ = 0.3236 ($wR_2$ all data = 0.3606), gof = 1.228, $_{max}$ = 59.311°. CCDC 1954948.

## 2.11. [{Co(**2**)(NCS)$_2$}·0.8MeOH·1.8CHCl$_3$]$_n$

$C_{50.6}H_{49}Cl_{5.4}CoN_8O_{2.8}S_2$, $M_r$ = 1128.46, orange plate, monoclinic, space group *C*2/*c*, *a* = 37.7611(9), *b* = 17.3396(3), *c* = 27.5031(6) Å, *β* = 135.1980(10)°, *V* = 12689.5(5) Å$^3$, $D_c$ = 1.181 g cm$^{-3}$, *T* = 130 K, *Z* = 8, *Z'* = 1, µ(GaKα) = 3.447 mm$^{-1}$. Total 91,813 reflections, 12996 unique ($R_{int}$ = 0.1323). Refinement of 8243 reflections (655 parameters) with *I* > 2*σ*(*I*) converged at final $R_1$ = 0.1424 ($R_1$ all data = 0.1884), $wR_2$ = 0.4180 ($wR_2$ all data = 0.5084), gof = 0.918, $_{max}$ = 57.448°. CCDC 1954949.

## 3. Results and Discussion

### 3.1. Synthesis and Characterization of Ligands **1** and **2**

The strategy for the preparation of compounds **1** and **2** was similar to that used to synthesize related tetratopic ligands [11] and is adapted from a procedure reported in the literature [38]. The route is summarized in Scheme 5. MALDI-TOF mass spectra of **1** and **2** are shown in Figures S3 and S4 (see Supplementary material). The base peak in both spectra arises from the [M+H]$^+$ ion (*m*/*z* = 741.34 for compound **1**, and *m*/*z* = 713.41 for compound **2**).



**1**  R = CH$_2$CHEtCH$_2$CH$_3$
**2**  R = CH$_2$CH$_2$CHMeCH$_3$
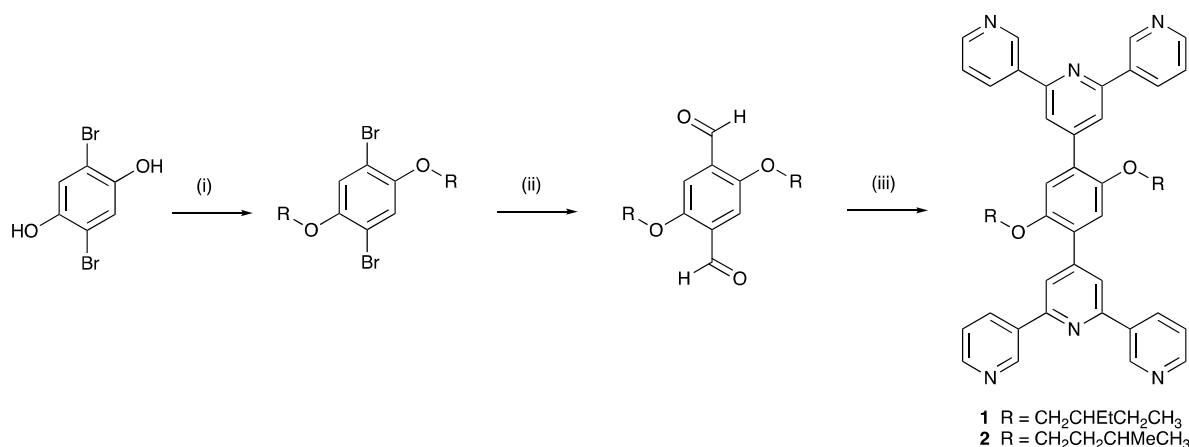
**Scheme 5.** Synthetic route to **1** and **2**. Conditions (see Materials and Methods for full details): (i) RBr, anhydrous K$_2$CO$_3$, dry DMF, 100 °C, 18 h; (ii) $^n$BuLi, Et$_2$O, 0 °C; dry DMF, warmed to room temperature, 17 h. (iii) 3-acetylpyridine, KOH, EtOH, aqueous NH$_3$, room temperature, three days for **1** and one day for **2**.

The $^1$H and $^{31}$C{$^1$H} NMR spectra of **1** and **2** were recorded in CDCl$_3$ and signals were assigned using the COSY, NOESY, HMQC and HMBC spectra. The spectroscopic signatures of the tpy domains are not affected by the change in the alkoxy substituent, and the aliphatic regions of the spectra are consistent with the 2-ethylbutoxy and 3-methylbutoxy groups in **1** and **2**, respectively (Figure 1). HMQC and HMBC spectra of the two compounds are shown in Figures S5–S8 (see Supplementary material). The solution absorption spectra of compounds **1** and **2** are displayed in Figure 2 and are similar to that observed for 1,4-bis(*n*-octyloxy)-2,5-bis(3,2':6',3''-terpyridin-4'-yl)benzene [13]. Absorptions arise from spin-allowed π*←π and π*←*n* transitions.
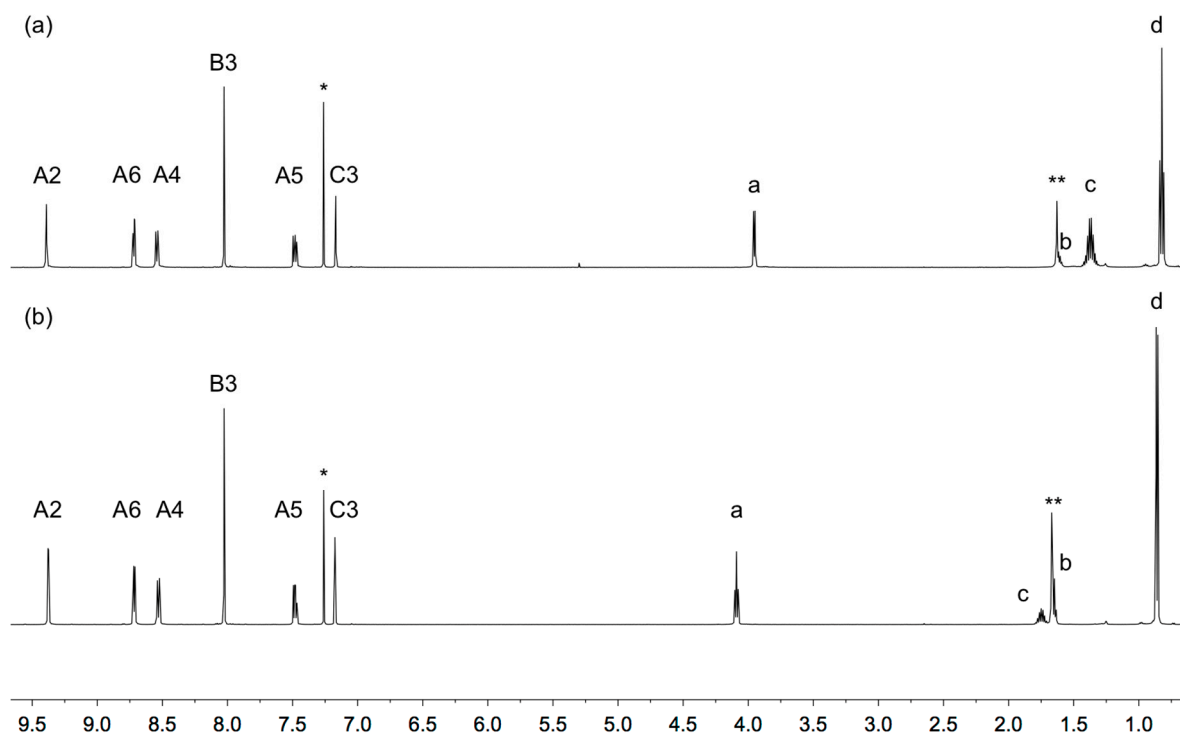
**Figure 1.** $^1$H NMR (500 MHz, CDCl$_3$, 298 K) of (**a**) **1** and (**b**) **2**. Chemical shifts in $\delta$/ppm. * = CHCl$_3$, ** = water.
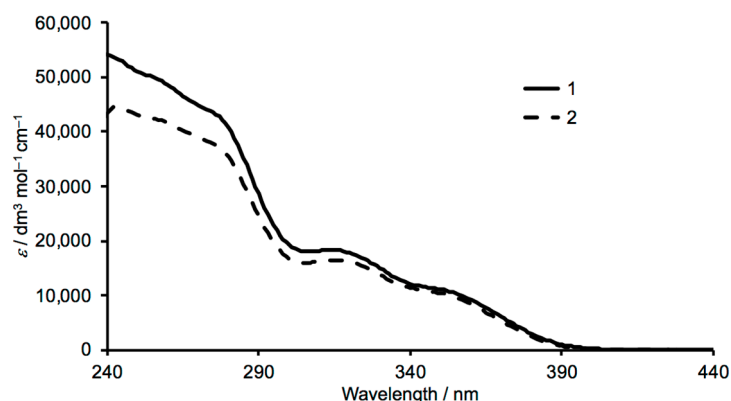


**Figure 2.** Solution absorption spectra of **1** and **2** in CHCl$_3$ ($1.2 \times 10^{-5}$ mol dm$^{-3}$ for **1**, $1.0 \times 10^{-5}$ mol dm$^{-3}$ for **2**).

### 3.2. Crystal Growth and Powder X-ray Diffraction

Single crystals of [{Co(**1**)(NCS)$_2$}·MeOH·3CHCl$_3$]$_n$ and [{Co(**2**)(NCS)$_2$}·0.8MeOH·1.8CHCl$_3$]$_n$ were grown under ambient conditions by layering a methanol solution of Co(NCS)$_2$ over a chloroform solution of ligand **1** or **2**. After selection of crystals for single-crystal X-ray diffraction studies (see Section 3.2), the bulk materials were analyzed by powder X-ray diffraction (PXRD). Despite careful handling of the crystals, loss of solvent could not be prevented completely, and as a result, the PXRD spectra were of poor quality. Figure 3 shows a refinement of the PXRD pattern for each bulk material compared with that determined from the single crystal structure of each of [{Co(**1**)(NCS)$_2$}·MeOH·3CHCl$_3$]$_n$ and [{Co(**2**)(NCS)$_2$}·0.8MeOH·1.8CHCl$_3$]$_n$. The profile matching refinement confirmed that the single crystal structures of [{Co(**2**)(NCS)$_2$}·0.8MeOH·1.8CHCl$_3$]$_n$ and [{Co(**1**)(NCS)$_2$}·MeOH·3CHCl$_3$]$_n$ are representative of the bulk sample and the main phase of the bulk sample, respectively. Minor phases observed in the PXRD spectrum of the bulk material of

[{Co(**1**)(NCS)$_2$}·MeOH·3CHCl$_3$]$_n$ could not be assigned and most likely appear as a consequence of solvent loss during sample preparation and measurement.
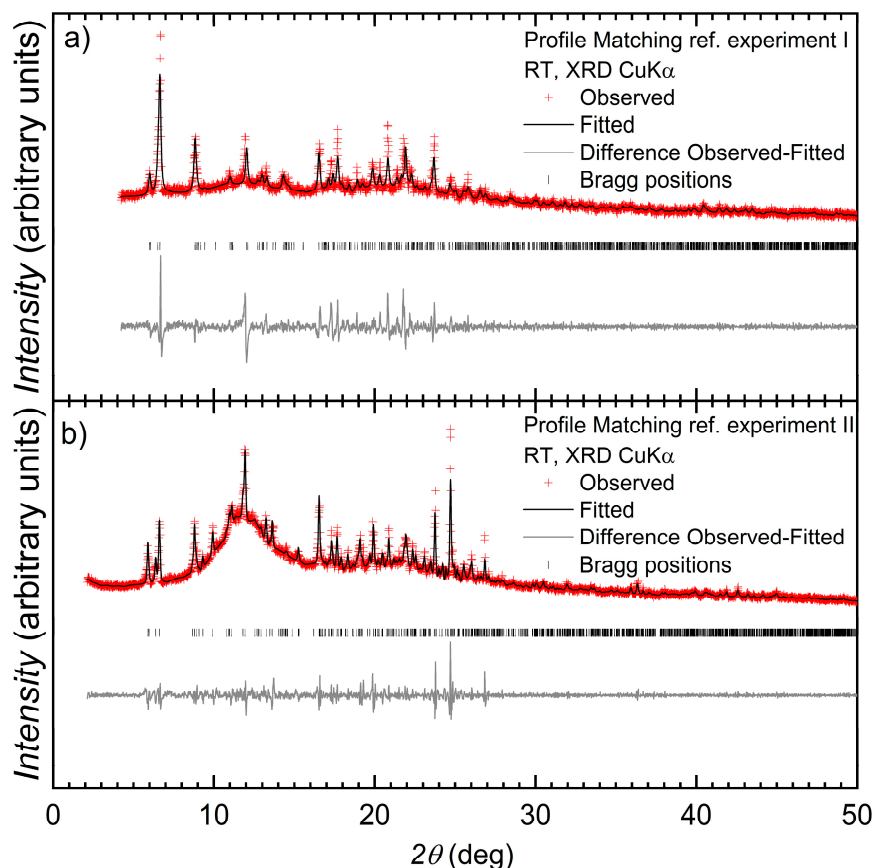


**Figure 3.** Laboratory X-ray diffraction (CuKα1 radiation) pattern (red crosses) of [{Co(**1**)(NCS)$_2$}·MeOH·3CHCl$_3$]$_n$ (experiment I) and [{Co(**2**)(NCS)$_2$}·0.8MeOH·1.8CHCl$_3$]$_n$ (experiment II) (space group *C2/c*, No. 15) at room temperature. The black line corresponds to the best fit from the profile matching refinement. Lower vertical marks denote the Bragg peak positions for [{Co(**1**)(NCS)$_2$}·MeOH·3CHCl$_3$]$_n$ and [{Co(**2**)(NCS)$_2$}·0.8MeOH·1.8CHCl$_3$]$_n$ phases. The bottom grey line represents the difference between experimental and calculated points.

### 3.3. Single Crystal Structures

Ligands **1** and **2** react with Co(NCS)$_2$ to form structurally similar three-dimensional networks [{Co(**1**)(NCS)$_2$}·MeOH·3CHCl$_3$]$_n$ and [{Co(**2**)(NCS)$_2$}·0.8MeOH·1.8CHCl$_3$]$_n$. The change from the 2-ethylbutoxy to 3-methylbutoxy substituents on the central phenylene spacer in the ligand has little impact on the structural assembly. Both compounds crystallize in the *C2/c* space group with similar cell dimensions (see Sections 2.10 and 2.11). We therefore discuss only one structure in detail. In [{Co(**2**)(NCS)$_2$}·0.8MeOH·1.8CHCl$_3$]$_n$, the 3-methylbutoxy chains are disordered and were modelled using restraints. The structure chosen for the detailed discussion is therefore [{Co(**1**)(NCS)$_2$}·MeOH·3CHCl$_3$]$_n$. The asymmetric unit contains two independent cobalt atoms and two independent half-ligands **1** (Figure S9), and the second half of each ligand is generated by inversion. Atom Co1 resides on an inversion centre (Wyckoff notation *n*), while Co2 lies on a 2-fold axis. Figure 4 shows the repeat unit of the coordination network with symmetry-generated atoms, and bond distances for the coordination spheres of Co1 and Co2 are given in Table 1. All bond lengths are typical. Both atoms Co1 and Co2 are octahedrally coordinated with *trans*-arrangements of thiocyanato ligands, and N–Co–N bond angles lie in the 87.0(2)° to 93.1(3)° range. Each metal atom binds to one pyridine donor atom of four different ligands **1**, thereby acting as a 4-connecting

node. For comparison, the asymmetric unit and repeat unit in $[\{Co(\mathbf{2})(NCS)_2\}\cdot 0.8MeOH\cdot 1.8CHCl_3]_n$ are depicted in Figures S10 and S11.
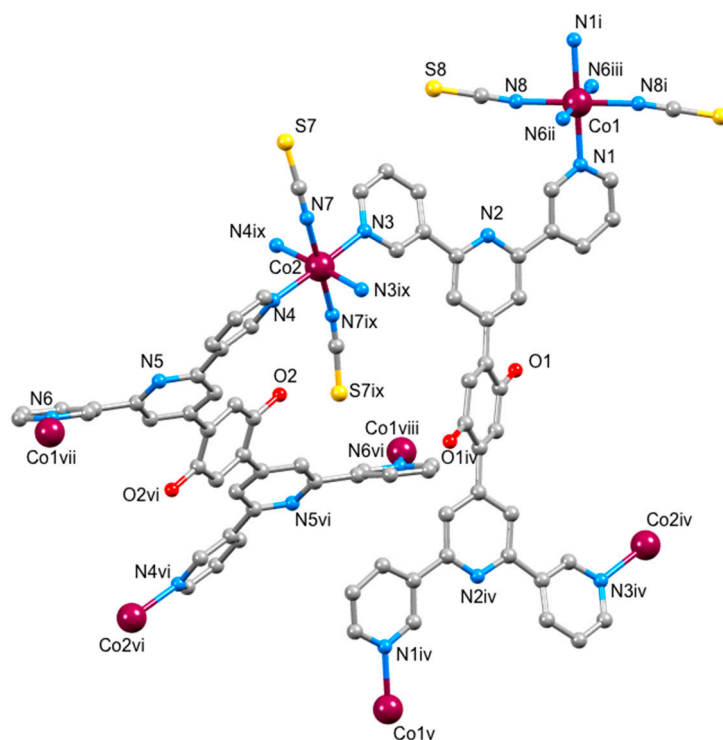


**Figure 4.** The repeat unit in the coordination network of $[\{Co(\mathbf{1})(NCS)_2\}\cdot MeOH\cdot 3CHCl_3]_n$ with symmetry-generated atoms. For clarity, H atoms and solvent molecules are omitted, and only the O atoms of the alkoxy groups are shown. Symmetry codes: i = $^1/_2 - x$, $^1/_2 - y$, $-z$; ii = $1 - x$, $-1 + y$, $^1/_2 - z$; iii = $-^1/_2 + x$, $^3/_2 - y$, $-^1/_2 + z$; iv = $1 - x$, $1 - y$, $1 - z$; v = $^1/_2 + x$, $^1/_2 + y$, $1 + z$; vi = $1 - x$, $2 - y$, $1 - z$; vii = $1 - x$, $1 + y$, $^1/_2 - z$; viii = $^1/_2 - x$, $^1/_2 + y$, $^1/_2 - z$; ix = $1 - x$, $y$, $^1/_2 - z$. For an ORTEP-style figure of the asymmetric unit, see Figure S9 in the Supplementary material.

**Table 1.** Important bond lengths in $[\{Co(\mathbf{1})(NCS)_2\}\cdot MeOH\cdot 3CHCl_3]_n$ and $[\{Co(\mathbf{2})(NCS)_2\}\cdot 0.8MeOH\cdot 1.8CHCl_3]_n$.

| Bond [a] | $[\{Co(\mathbf{1})(NCS)_2\}\cdot MeOH\cdot 3CHCl_3]_n$ | Corresponding Bond Lengths in $[\{Co(\mathbf{2})(NCS)_2\}\cdot 0.8MeOH\cdot 1.8CHCl_3]_n$ |
|---|---|---|
| | Bond Length/Å | Bond Length/Å |
| Co1–N1 | 2.171(6) | 2.175(6) |
| Co1–N6 [ii] | 2.229(6) | 2.244(6) |
| Co1–N8 | 2.065(6) | 2.091(5) |
| Co2–N3 | 2.136(6) | 2.138(6) |
| Co2–N4 | 2.145(6) | 2.134(6) |
| Co2–N7 | 2.074(6) | 2.107(7) |

[a] In $[\{Co(\mathbf{1})(NCS)_2\}\cdot MeOH\cdot 3CHCl_3]_n$, symmetry code ii = $1 - x$, $-1 + y$, $\frac{1}{2} - z$ (see Figure 4). In $[\{Co(\mathbf{2})(NCS)_2\}\cdot 0.8MeOH\cdot 1.8CHCl_3]_n$, symmetry code ii = $x$, $1 - y$, $-^1/_2 + z$ (see Figure S11).

The tpy unit of each independent ligand **1** is twisted to give a conformation close to conformation III in Scheme 1. Coordination occurs only through the two outer nitrogen atoms (see the discussion in the introduction). Angles between the least squares planes through pairs of pyridine rings containing N1/N2, N2/N3, N4/N5 and N5/N6 are 10.6(4), 18.6(4), 29.8(3) and 36.1(3)°, respectively. The phenylene ring is twisted 39.1(3)° with respect to the pyridine ring to which it is bonded in one independent ligand **1** and 38.8(3)° in the other. These values are typical for bonded aromatic rings.

The structure propagates into a three-dimensional network which possesses four chemically distinct nodes, all of which are 4-connecting. These nodes are defined by atoms Co1 and Co2 and the centroids of the two independent phenylene rings. The two ligand nodes are topologically equivalent (this was confirmed using the program Systre [39]) and thus the underlying topological net is trinodal. The full vertex symbol is $(6^2.8^4)(6^4.8^2)(6^5.8)_2$, with the individual symbols referring to Co1, Co2 and the ligands, respectively. Figure 5 displays part of the net viewed down the *a*- and *c* axes. A view down the *b*-axis is shown in Figure S12. In these representations, Co1 atoms are shown in blue, Co2 in orange, and the ligand nodes in green. Combination of Co2 and ligand nodes generates sheets that are coplanar with the *bc*-plane, while sheets composed of Co1 and ligand nodes slice obliquely through the unit cell. The net is self-penetrating, with the shortest circuits of the net penetrated by rods of the same net [40], and is highly unusual, with the net not appearing on the Reticular Chemistry Structure Resource (RCSR) database of 3D nets [41]. The self-penetration can be appreciated by inspection of Figure 6. The catenated shortest circuits comprise four Co1 atoms linked by ligand nodes, and three such circuits are depicted in red and magenta in Figure 6. This representation highlights the interlocking of the shortest circuits which produces the self-penetrating $(6^2.8^4)(6^4.8^2)(6^5.8)_2$ net.



**(a)**　　　　　　　　　　　　　　　　**(b)**
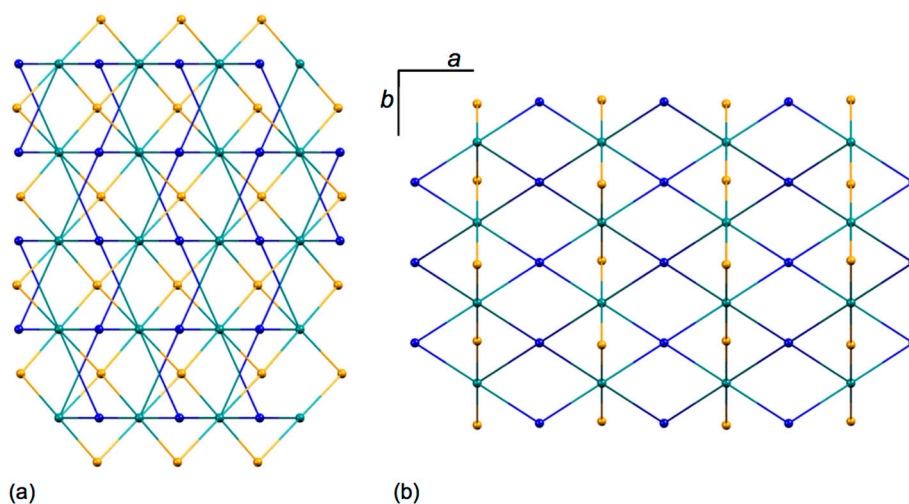
**Figure 5.** Part of the 3D net in $[\{Co(\mathbf{1})(NCS)_2\}\cdot MeOH\cdot 3CHCl_3]_n$ viewed down the crystallographic (**a**) *a*-axis and (**b**) *c*-axis. Colour code for the nodes: Co1 blue, Co2 orange, ligand centroids green.
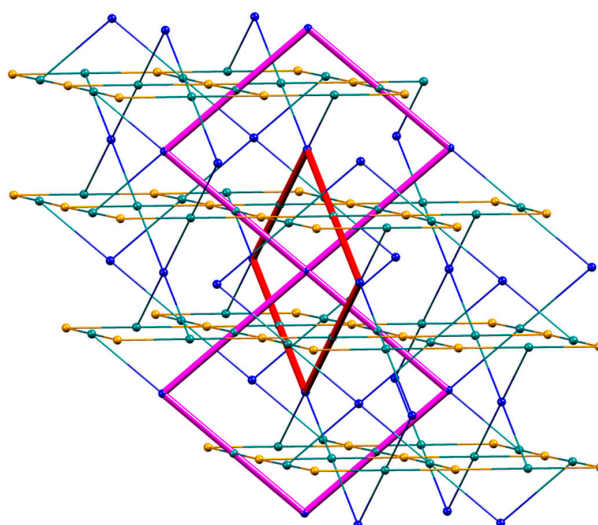


**Figure 6.** Part of the 3D net in $[\{Co(\mathbf{1})(NCS)_2\}\cdot MeOH\cdot 3CHCl_3]_n$ highlighting the interlocking of the shortest circuits (shown in red and magenta). Colour code for the nodes: Co1 blue, Co2 orange, ligand centroids green.

The structural similarity between the nets in [{Co(**1**)(NCS)$_2$}·MeOH·3CHCl$_3$]$_n$ and [{Co(**2**)(NCS)$_2$}·0.8MeOH·1.8CHCl$_3$]$_n$ indicates that both the 2-ethylbutoxy and 3-methylbutoxy groups are accommodated within the cavities in the network and that there is little difference between the steric requirements of these substituents. Significantly, if the substituents are replaced by *n*-octyloxy chains in [{Co(**3**)(NCS)$_2$}·4CHCl$_3$]$_n$ where **3** is 1,4-bis(*n*-octyloxy)-2,5-bis(3,2':6',3''-terpyridin-4'-yl)benzene, a switch in assembly is observed to an {4$^2$.8$^4$} *lvt* net [13]. In this structure, the long *n*-octyloxy chains are in non-extended conformations and each lies over a 3,2':6',3''-tpy unit with close C–H...π contacts.

## 4. Conclusions

We have described the synthesis and characterization of the tetratopic bis(3,2':6',3''-tpy) ligands **1** and **2**. Reactions of **1** and **2** with Co(NCS)$_2$ under ambient conditions lead to the assembly of [{Co(**1**)(NCS)$_2$}·MeOH·3CHCl$_3$]$_n$ and [{Co(**2**)(NCS)$_2$}·0.8MeOH·1.8CHCl$_3$]$_n$, the structures of which are similar. Each exhibits an unusual trinodal, self-penetrating (6$^2$.8$^4$)(6$^4$.8$^2$)(6$^5$.8)$_2$ 3D-net with the nodes defined by two independent cobalt centres, and the centroids of two crystallographically independent but topologically equivalent ligands. PXRD confirms that the single crystal structures are representative of the bulk material. The similar steric requirements of the 2-ethylbutoxy and 3-methylbutoxy substituents leads to a reproducible 3D-assembly, contrasting with the assembly of a 3D {4$^2$.8$^4$} net when *n*-octyloxy substituents replace the 2-ethylbutoxy and 3-methylbutoxy groups. We will now further explore how choice of substituents leads to a switch in network.

## References

1. Constable, E.C. The Coordination Chemistry of 2,2':6',2''-Terpyridine and Higher Oligopyridines. *Adv. Inorg. Chem. Radiochem.* **1986**, *30*, 69–121. [CrossRef]

2. Constable, E.C. 2,2':6',2''-Terpyridines: From chemical obscurity to common supramolecular motifs. *Chem. Soc. Rev.* **2007**, *36*, 246–253. [CrossRef] [PubMed]

3. Constable, E.C.; Housecroft, C.E. More hydra than Janus – Non-classical coordination modes in complexes of oligopyridine liigands. *Coord. Chem. Rev.* **2017**, *359*, 84–104. [CrossRef]

4. Constable, E.C.; Housecroft, C.E. Tetratopic bis(4,2':6',4''-terpyridine) and bis(3,2':6',3''-terpyridine) ligands as 4-connecting nodes in 2D-coordination networks and 3D-frameworks. *J. Inorg. Organomet. Polym. Mater.* **2018**, *28*, 414–427. [CrossRef]

5. Wild, A.; Winter, A.; Schluetter, F.; Schubert, U.S. Advances in the Field of π-Conjugated 2,2':6',2''-Terpyridines. *Chem. Soc. Rev.* **2011**, *40*, 1459–1511. [CrossRef]

6. Yan, Y.; Huang, J. Hierarchical Assemblies of Coordination Supramolecules. *Coord. Chem. Rev.* **2010**, *254*, 1072–1080. [CrossRef]

7. Constable, E.C. A Journey from Supramolecular Chemistry to Nanoscale Networks. *Chimia* **2013**, *67*, 388–392. [CrossRef]

8. Constable, E.C.; Ward, M.D. Synthesis and co-ordination behaviour of 6',6''-bis(2-pyridyl)-2,2':4,4'':2'',2'''-quaterpyridine; 'back-to-back' 2,2':6',2''-terpyridine. *J. Chem. Soc. Dalton Trans.* **1990**, 1405–1409. [CrossRef]

9.  Newkome, G.R.; Cardullo, F.; Constable, E.C.; Moorefield, C.N.; Cargill Thompson, A.M.W. Metallomicellanols: Incorporation of ruthenium(II) - 2,2′:6′,2″-terpyridine triads into cascade polymers. *J. Chem. Soc. Chem. Commun.* **1993**, 925–927. [CrossRef]

10. Fu, J.-H.; Wang, S.-Y.; Chen, Y.-S.; Prusty, S.; Chan, Y.-T. One-Pot Self-Assembly of Stellated Metallo-Supramolecules from Multivalent and Complementary Terpyridine-Based Ligands. *J. Am. Chem. Soc.* **2019**. [CrossRef]

11. Lü, J.; Han, L.-W.; Alsmail, N.H.; Blake, A.J.; Lewis, W.; Cao, R.; Schröder, M. Control of Assembly of Dihydropyridyl and Pyridyl Molecules via Directed Hydrogen Bonding. *Cryst. Growth Des.* **2015**, *15*, 4219–4224. [CrossRef] [PubMed]

12. Lü, J.; Perez-Krap, C.; Suyetin, M.; Alsmail, N.H.; Yan, Y.; Yang, S.; Lewis, W.; Bicjoutskaia, E.; Tang, C.C.; Blake, A.J.; et al. Polycatenated 2D Hydrogen-Bonded Binary Supramolecular Organic Frameworks (SOFs) with Enhanced Gas Adsorption and Selectivity. *Cryst. Growth Des.* **2018**, *18*, 2555–2562. [CrossRef] [PubMed]

13. Klein, Y.M.; Constable, E.C.; Housecroft, C.E.; Prescimone, A. A 3-dimensional {42.84} lvt net built from a ditopic bis(3,2′:6′,3″-terpyridine) tecton bearing long alkyl tails. *CrystEngComm* **2015**, *17*, 2070–2073. [CrossRef]

14. Klein, Y.M.; Prescimone, A.; Constable, E.C.; Housecroft, C.E. A double-stranded 1D-coordination polymer assembled using the tetravergent ligand 1,1′-bis(4,2′:6′,4″-terpyridin-4′-yl)ferrocene. *Inorg. Chem. Comm.* **2016**, *70*, 118–120. [CrossRef]

15. Klein, Y.M.; Prescimone, A.; Karpacheva, M.; Constable, E.C.; Housecroft, C.E. Sometimes the same, sometimes different: Understanding self-assembly algorithms in coordination networks. *Polymers* **2018**, *10*, 1369. [CrossRef] [PubMed]

16. Constable, E.C.; Housecroft, C.E.; Vujovic, S.; Zampese, J.A. 2D→2D Parallel interpenetration of (4,4) sheets constructed from a ditopic bis(4,2′:6′,4″-terpyridine). *CrystEngComm* **2014**, *16*, 3494–3497. [CrossRef]

17. Vujovic, S. Constable, E.C.; Housecroft, C.E.; Morris, C.D.; Neuburger, M.; Prescimone, A. Engineering 2D→2D parallel interpenetration using long alkoxy-chain substituents. *Polyhedron* **2015**, *92*, 77–83. [CrossRef]

18. Klein, Y.M.; Prescimone, A.; Neuburger, M.; Constable, E.C.; Housecroft, C.E. What a difference a tail makes: 2D→2D parallel interpenetration of sheets to interpenetrated nbo networks using ditopic-4,2′:6′,4″-terpyridine ligands. *CrystEngComm* **2017**, *19*, 2894–2902. [CrossRef]

19. Cave, G.W.V.; Raston, C.L. Efficient synthesis of pyridine *via* a sequential solventless aldol condensation and Michael addition. *J. Chem. Soc. Perkin Trans. 1* **2001**, 3258–3264. [CrossRef]

20. Beddoe, S.V.F.; Fitzpatrick, A.J.; Price, J.R.; Mallo, N.; Beves, J.E.; Morgan, G.G.; Kitchen, J.A.; Keene, T.D. A Bridge Too Far: Testing the Limits of Polypyridyl Ligands in Bridging Soluble Subunits of a Coordination Polymer. *Cryst. Growth Des.* **2017**, *17*, 6603–6612. [CrossRef]

21. Housecroft, C.E.; Constable, E.C. Ditopic and tetratopic 4,2′:6′,4″-Terpyridines as Structural Motifs in 2D- and 3D-Coordination Assemblies. *Chimia* **2019**, *73*, 462–467. [CrossRef]

22. Yoshida, J.; Nishikiori, S.; Hidetaka, Y. Bis(3-cyano-pentane-2,4-dioato) Co(II) as a Linear Building Block for Coordination Polymers: Combinations with Two Polypyridines. *J. Coord. Chem.* **2013**, *66*, 2191–2200. [CrossRef]

23. Shao, P.; Li, Z.; Luo, J.; Wang, H.; Qin, J. A Convenient Synthetic Route to 2,5-Dialkoxyterephthalaldehyde. *Synth. Commun.* **2005**, *35*, 49–53. [CrossRef]

24. Jin, J.-Y.; Jin, Z.-Z.; Xia, Y.; Zhou, Z.-Y.; Wu, X.; Zhu, D.-X.; Su, Z.-M. Design and synthesis of 1,4-bis[4-(1,1-dicyanovinyl)styryl]-2,5-bis(alkoxy)benzenes as red organic electroluminescent PPV analogs. *Polymer* **2007**, *48*, 4028–4033. [CrossRef]

25. *Software for the Integration of CCD Detector System Bruker Analytical X-ray Systems, version 2*; Bruker AXS: Madison, WI, USA, 2013.

26. Sheldrick, G.M. ShelXT-Integrated space-group and crystal-structure determination. *Acta Cryst.* **2015**, *A71*, 3–8. [CrossRef] [PubMed]

27. Dolomanov, O.V.; Bourhis, L.J.; Gildea, R.J.; Howard, J.A.K.; Puschmann, H. Olex2: A Complete Structure Solution, Refinement and Analysis Program. *J. Appl. Cryst.* **2009**, *42*, 339–341. [CrossRef]

28. Sheldrick, G.M. Crystal Structure Refinement with ShelXL. *Acta Cryst.* **2015**, *C27*, 3–8. [CrossRef]

29. Palatinus, L.; Chapuis, G. Superflip - A Computer Program for the Solution of Crystal Structures by Charge Flipping in Arbitrary Dimensions. *J. Appl. Cryst.* **2007**, *40*, 786–790. [CrossRef]

30. Palatinus, L.; Prathapa, S.J.; van Smaalen, S. EDMA: A Computer Program for Topological Analysis of Discrete Electron Densities. *J. Appl. Cryst.* **2012**, *45*, 575–580. [CrossRef]

31. Macrae, C.F.; Edgington, P.R.; McCabe, P.; Pidcock, E.; Shields, G.P.; Taylor, R.; Towler, M.; van de Streek, J. Mercury: Visualization and Analysis of Crystal Structures. *J. Appl. Cryst.* **2006**, *39*, 453–457. [CrossRef]

32. Macrae, C.F.; Bruno, I.J.; Chisholm, J.A.; Edgington, P.R.; McCabe, P.; Pidcock, E.; Rodriguez-Monge, L.; Taylor, R.; van de Streek, J.; Wood, P.A. Mercury CSD 2.0 - New Features for the Visualization and Investigation of Crystal Structures. *J. Appl. Cryst.* **2008**, *41*, 466–470. [CrossRef]

33. Spek, A.L. Platon Squeeze: A Tool for the Calculation of the Disordered Solvent Contribution to the Calculated Structure Factors. *Acta Crystallogr. Sect. C Struct. Chem.* **2015**, *71*, 9–18. [CrossRef] [PubMed]

34. LeBail, A.; Duroy, H.; Fourquet, J.L. Ab-initio structure determination of $LiSbWO_6$ by X-ray powder diffraction. *Mat. Res. Bull.* **1988**, *23*, 447–452. [CrossRef]

35. Pawley, G.S. Unit-cell refinement from powder diffraction scans. *J. Appl. Cryst.* **1981**, *14*, 357–361. [CrossRef]

36. Rodríguez-Carvajal, J. Recent Advances in Magnetic Structure Determination by Neutron Powder Diffraction. *Phys. B* **1993**, *192*, 55–69. [CrossRef]

37. Roisnel, T.; Rodríguez-Carvajal, J. WinPLOTR: A Windows tool for powder diffraction patterns analysis. *Mater. Sci. Forum* **2001**, 118–123. [CrossRef]

38. Prasad, T.K.; Suh, M.P. Metal-organic frameworks incorporating various alkoxy pendant groups: Hollow tubular morphologies, X-ray single-crystal structures, and selective carbon dioxide adsorption properties. *Chem. Asian J.* **2015**, *10*, 2257–2263. [CrossRef]

39. Delgado-Friedrichs, O.; O'Keeffe, M. Identification of and symmetry computation for crystal nets. *Acta Crystallogr. Sect. A* **2003**, *59*, 351–360. [CrossRef]

40. Batten, S.R.; Neville, S.M.; Turner, D.R. *Coordination Polymers: Design, Analysis and Application*; RSC Publishing: Cambridge, UK, 2009; ISBN 978-0-85404-837-3.

41. O'Keeffe, M.; Peskov, M.A.; Ramsden, S.J.; Yaghi, O.M. The Reticular Chemistry Structure Resource (RCSR) database of, and symbols for, crystal nets. *Acc. Chem. Res.* **2008**, *41*, 1782–1789. [CrossRef]